Phase Behaviors of Mainchain Liquid Crystals. ²H NMR and Pressure–Volume–Temperature Analysis of Dimer and Trimer Model Compounds

Akihiro ABE, Takanori TAKEDA, Toshihiro HIEJIMA,
and Hidemine FURUYA*

*Department of Industrial Chemistry, Tokyo Institute of Polytechnics,
1583 Iiyama, Atsugi 243–0297, Japan*
** Department of Polymer Chemistry, Tokyo Institute of Technology,
Ookayama, Meguro-ku, Tokyo 152–8552, Japan*

(Received February 16, 1999)

ABSTRACT: Our previous studies on the structure–property relation of dimer liquid crystals (LC), α,ω-bis(4-cyanobiphenyl-4'-yloxy)alkanes (CBA-n, $n=9$, 10), have been extended to include trimer compounds, 4,4'-bis[ω-(4-cyanobiphenyl-4'-yloxy)alkoxy]biphenyls (CBA-Tn, $n=9,10$), comprising three mesogenic units jointed by two intervening spacers. These nematic-LC-forming compounds were chosen as a model for the mainchain-type polymer LCs on the assumption that the spatial configuration and thermodynamic roles of the flexible spacer are nearly identical as long as the chemical structure of the repeating unit is similar. The ²H NMR method was extensively used to elucidate the orientational characteristics of these molecules in the mesophase. The analysis of binary mixtures with a low molar mass (monomer) LC gave an important information regarding the mesophase structure of CBA-Tn as well as CBA-n. The pressure–volume–temperature (PVT) relation was determined to estimate the constant–volume transition entropies at the interphase such as crystal/nematic LC/isotropic melt. The results were found to be favorably compared with the conformational entropy changes derived on the basis of the rotational isomeric state analysis of the ²H NMR data. Finally, an important role of the flexible spacer was emphasized in determining the molecular ordering as well as thermodynamic properties of mainchain-type LCs.
   KEY WORDS   Dimer Liquid Crystals / Trimer Liquid Crystals / Orientational Order / Nematic
Conformation / Constant–Volume Transition Entropy / Conformational Entropy /

In a series of papers,[1–7] we have extensively studied orientational ordering and pressure–volume–temperature (PVT) properties of dimer liquid crystals (LC) having structures such as

CN—⟨◯⟩—⟨◯⟩—O(CH₂)ₙO—⟨◯⟩—⟨◯⟩—CN
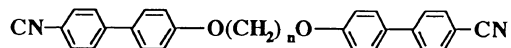
α,ω-Bis(4-cyanobiphenyl-4'-yloxy)alkanes (CBA-n)
       CBA-9:   C 134.8 N 173.0   I (°C)
       CBA-10:   C 164.6 N 184.0   I (°C)

where suffix n designate the number of carbon atoms in the spacer. CBA-9 and -10 exhibit two well-defined phase transitions as a function of temperature: crystal (C) ↔ nematic LC (N) ↔ isotropic melt (I). These ether-type LCs are known to exhibit a pronounced odd–even characteristics in various thermodynamic quantities at the NI phase boundaries,[8] indicating that the spatial configuration of the spacer plays a significant role.[9] The thermal pressure coefficient γ ($=\alpha/\beta$) was estimated at around the phase transition point from the observed thermal expansion coefficient α and compressibility β. The phase-transition entropy observed under constant pressure $(\Delta S_{tr})_p$ was then corrected for contribution ΔS_v from the volume change, leading to an estimate of the constant-volume transition entropy $(\Delta S_{tr})_v$ according to a conventional thermodynamic relation[10,11]:

$$(\Delta S_{tr})_v = (\Delta S_{tr})_p - \Delta S_v \qquad (1)$$

and

$$\Delta S_v = \gamma \Delta V_{tr} \qquad (2)$$

where ΔV_{tr} is the volume change at the transition. These relations can be applied to both CN and NI transitions,

and thus subscript tr is used in place of cn or ni. The values of $(\Delta S_{tr})_v$ thus estimated for the aforementioned systems were favorably compared with the conformational entropies of the spacer calculated from the spatial arrangements elucidated spectroscopically in the two relevant states.

On the other hand, molecular weight dependence of $(\Delta S_{ni})_p$ has been studied by Blumstein *et al.*[14] for mainchain LC polymers, poly(4,4'-dioxy-2,2'-dimethylazoxybenzene-dodecanedioyl) (known as DDA-9). When the unit of $(\Delta S_{ni})_p$ is expressed by the entropy change per spacer, magnitude of $(\Delta S_{ni})_p$ becomes nearly invariant over a wide range from the dimer model compound (9-DDA-9) to polymers. These results strongly suggest that the spatial configuration of the flexible spacer and its thermodynamic roles remain nearly identical independent of the degree of polymerization. In order to test the validity of such supposition, studies were extended to include trimer LCs having homologous structures:

CN—⟨◯⟩—⟨◯⟩—O(CH₂)ₙO—⟨◯⟩—⟨◯⟩—O(CH₂)ₙO—⟨◯⟩—⟨◯⟩—CN
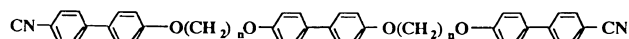
4,4'-Bis[ω-(4-cyanobiphenyl-4'-yloxy)alkoxy]biphenyls (CBA-Tn)
       CBA-T9:   C 146.0 N 195.7 I (°C)
       CBA-T10:   C 188.5 N 209.9 I (°C)

Following our previous studies,[4–6] samples deuterated at given sites were also prepared to elucidate ordering characteristics of molecules and the structure of mesophase by the ²H NMR method. For the purpose at hand, use of dimers and trimers having well-defined chemical structures is more preferable. Difficulties

associated with polymeric samples, *e.g.*, inhomogeneity in the degree of polymerization and enhanced transition temperatures, can be avoided.

Recently, Imrie and Luckhurst[15] have reported the results of an extensive work on a series of CBA-T*n* with *n* = 4 to 11. Comparison indicates that the transition temperatures T_{cn} and T_{ni} are similar between the two samples of *n* = 9 and 10. However, we did not observe any indication of a smectic phase on cooling at variance with their observation: (CBA-T9: 133°C and CBA-T10: 155°C).

EXPERIMENTAL

The preparation of CBA-T9 and -T10 has been reported previously.[16] Thermal transitions were measured with a TA Instruments modulated differential scanning calorimeter (DSC) calibrated with indium. Heating rates of 10 deg min^{-1} were employed in most of the DSC scans. The data were collected from the second-scan heating curves. Temperatures corresponding to the onset of phase transformation were recorded for each endotherm or exotherm. The numerical data thus obtained are shown above together with chemical structures.

The ^{2}H NMR spectra were recorded on a JEOL JNM-LA-500 spectrometer operating at 76.65 MHz deuterium resonance frequency and nonspinning mode. In the experiment, samples initially kept at a temperature above T_{ni} were cooled slowly to get into the nematic mesophase.

A *PVT* apparatus manufactured by GNOMIX Co. was used to determine the change in specific volume as a function of temperature and pressure. The apparatus consists of a bellows cell containing about 1—2 g of sample and mercury as a confining fluid. The deflection of the bellows under temperature and pressure changes is measured by a transformer. The volume change of the sample can be calculated by making allowance for the known *PVT* properties of mercury. In the isothermal mode, volume readings were recorded over a pressure range from 10 to 100 MPa at a fixed interval (10 MPa) while the temperature was kept invariant. The temperature was then changed by 10°C and the process repeated. The measurements were also performed in the isobaric mode (at 10 and 40 MPa) by ramping the temperature (30—250°C) up or down. Prior to the *PVT* measurements, the densities of the sample were determined with a pycnometer (volume *ca.* 50 mL) at 30°C under atmospheric pressure. About 2—3 g of sample was charged and calibration was carried out by using reagent grade ethanol. Density: CBA-T9, 1.172 g cm^{-3}; CBA-T10, 1.160 g cm^{-3}.

RESULTS AND DISCUSSION

Miscibility Test

Phase diagrams were constructed for a binary mixture to examine the compatibility of the dimer and trimer LCs by using DSC. The dimer and trimer molecules differ sizably in their contour length: 33—34 Å (CBA-*n*) and 56—58 Å (CBA-T*n*). The blends of two samples were prepared in chloroform solution, followed by evaporation of the solvent. In conformity with the polarizing
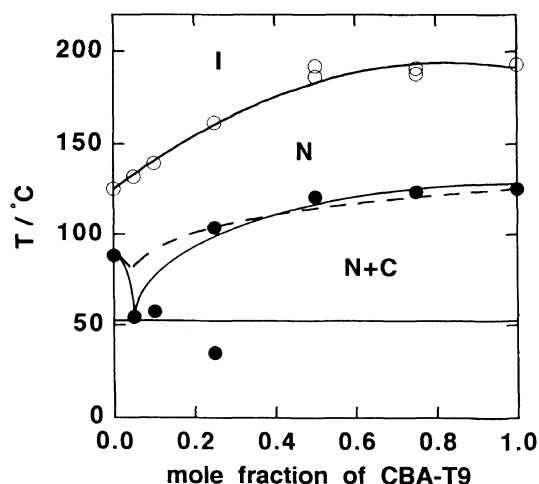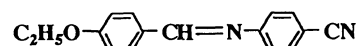

Figure 1. Phase diagram of a binary mixture comprising trimer CBA-T9 and monomer EBCA. Broken lines indicate phase boundaries calculated by the conventional Schröder-van Laar expression. The agreement was not much improved by adopting the Flory Huggins relation to take into account the molar volume effect.

microscopic observation, CBA-*n* and CBA-T*n* were found to be highly miscible with any combination of *n*. Examples of the phase diagram for mixtures CBA-9/CBA-T9 and CBA-10/CBA-T10 have been previously reported.[16] From the phase behavior, it is reasonable to assume that the nematic structure of the dimer and trimer LCs are similar for a given *n*. It is interesting to note here that the NI transition of a binary mixture takes place within a relatively narrow temperature region, and thus the width of the biphasic gap remains nearly unaltered over the entire concentration range.

Orientational Order and Structure of Mesophase

In a previous paper,[6] we have adopted the ^{2}H NMR analysis for binary mixtures comprising a low-molar-mass (monomer) LC and dimer LCs: *i.e.*, CBA-*n* dissolved in 4'-ethoxybenzilidene-4-cyanoaniline (EBCA).

$$C_2H_5O-\langle\bigcirc\rangle-CH=N-\langle\bigcirc\rangle-CN$$

4'-Ethoxybenzylidene-4-cyanoaniline (EBCA)
C 106.9   N 126.8   I   (°C)

The orientational order parameters S_{ZZ}^M of the mesogenic core were separately elucidated for the two components in given mixtures.

$$S_{ZZ}^M = (1/2)\langle 3\cos^2\theta - 1\rangle \tag{3}$$

where θ designates the tilt angle of the mesogenic core axis with respect to the domain director. The S_{ZZ}^M(CBA-*n*) *vs.* S_{ZZ}^M(EBCA) plot thus derived has provided some insight regarding the mesophase structure of dimer compounds. Following these treatments, we have examined the orientational characteristics of the components in the binary mixture CBA-T9/EBCA by preparing partially deuterated samples. The phase diagram for the mixture is illustrated in Figure 1. Since the NI transition temperature of CBA-T10 exceeds the guaranteed temperature limit (200°C) of our standard ^{2}H NMR probe, the measurement was not attempted for this sample. The deuterium quadrupolar splittings $\Delta\nu_c$ and $\Delta\nu_t$ were observed respectively for the central and
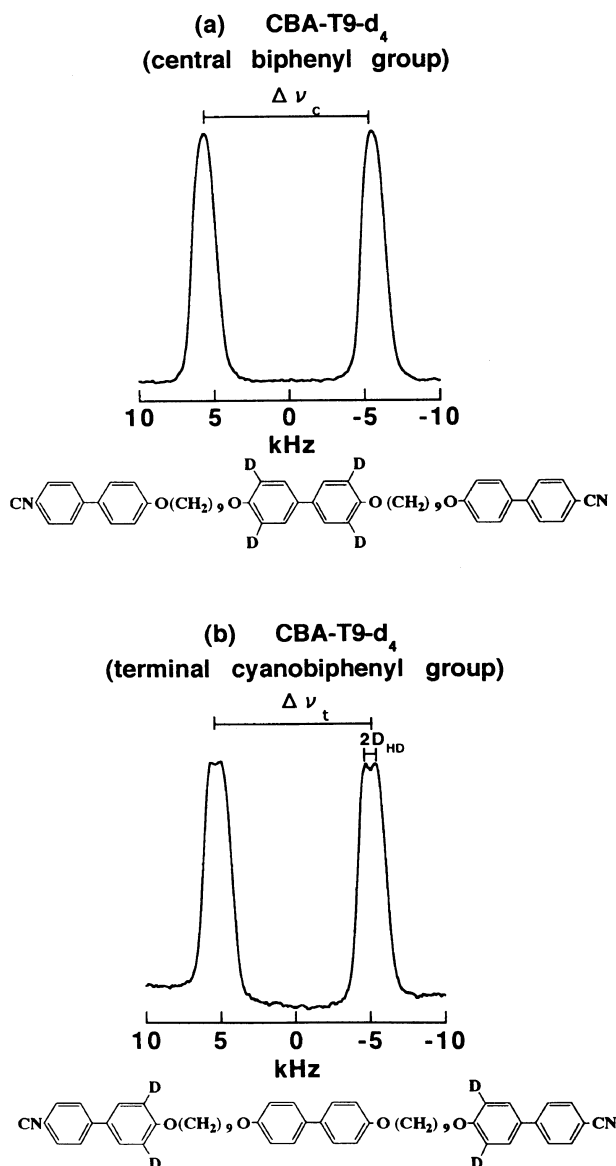
(a) CBA-T9-d₄
(central biphenyl group)

Δν_c

10 5 0 -5 -10
kHz

CN◇◇—O(CH₂)₉O—◇◇—O(CH₂)₉O—◇◇—CN

(b) CBA-T9-d₄
(terminal cyanobiphenyl group)

Δν_t

2D_HD

10 5 0 -5 -10
kHz

CN◇◇—O(CH₂)₉O—◇◇—O(CH₂)₉O—◇◇—CN

Figure 2. Examples of ^{2}H NMR spectra obtained for neat CBA-T9 at 192°C. The positions of the deuterium substitution are distinguished by the chemical structure for each diagram: (a) central mesogenic unit and (b) terminal mesogenic group. The orientational order parameter of the mesogenic core S_{ZZ}^M(CBA-T9, terminal) was deduced from the observed dipolar coupling (D_{HD}) and deuterium quadrupolar splitting ($\Delta\nu_t$).

terminal mesogenic units of the CBA-T9 component. Examples of the ^{2}H NMR spectra obtained for a neat CBA-T9 sample are shown in Figure 2. The splittings (D_{HD}) due to the dipolar coupling with the vicinal proton could be determined only for the terminal mesogenic units. The ratios of the two quadrupolar splittings $\Delta\nu_t/\Delta\nu_c$ were found to fall in the range of 0.95 ± 0.02 for most of the measurements, indicating that the orientational order of the cyanobiphenyl group at the terminal is slightly lower than that of the biphenyl group situated at the central part of CBA-T9. It should be noted here that the ratio remains invariant independent of temperature and concentration of CBA-T9 in the mixture, suggesting that the spatial configuration of the flexible spacer is stable as long as the molecule takes a nematic order. The orientational order parameters S_{ZZ}^M(CBA-Tn) and the associated biaxiality term S_{xx}-S_{yy} can be obtained
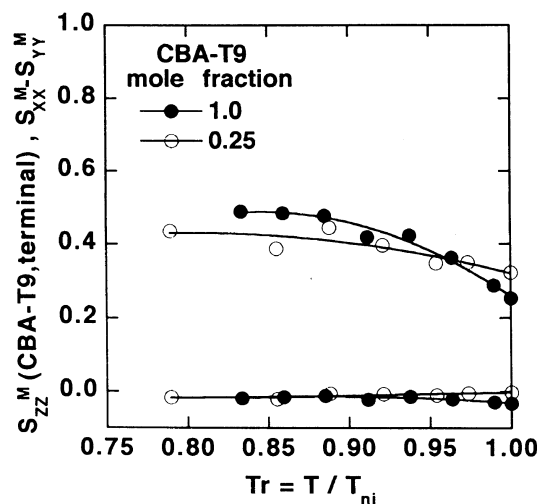

Figure 3. Variation of the order parameter of the mesogenic core S_{ZZ}^M(CBA-T9, terminal) and the associated biaxiality term S_{XX}^M—S_{YY}^M as a function of the reduced temperature $T_r = T/T_{ni}$: filled circles for neat CBA-T9 and open circles for CBA-T9 dissolved in EBCA (mole fraction 0.25).
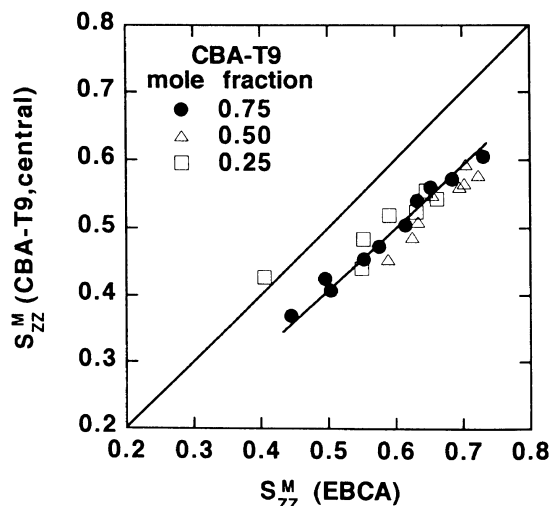

Figure 4. The order parameter S_{ZZ}^M(CBA-T9, central) of the central biphenyl group plotted against S_{ZZ}^M (EBCA) of the coexisting monomer LC. The former value was derived from the observed $\Delta\nu_c$ contribution from the biaxiality term being ignored. The data points were collected from binary mixtures of various compositions (0.75, 0.5, and 0.25 in terms of the mole fraction of CBA-T9) over a wide range of temperature. To facilitate comparison, the bisector is indicated.

for the terminal mesogenic unit from the observed splittings $\Delta\nu_t$ and D_{HD}.[6] The values of S_{ZZ}^M(CBA-Tn, terminal) thus obtained are plotted against the reduced temperature T_r ($= T/T_{ni}$) in Figure 3, where for an illustrative purpose, two extreme examples are shown: one for neat CBA-Tn and the other for a mixture with EBCA at the mole fraction of CBA-T9 = 0.25. The superposition principle nearly holds for the trimer as well as for the dimer. The contribution from the biaxiality term was found to remain insignificant throughout the measurements (cf. lower symbols in Figure 3). The corresponding plot S_{ZZ}^M(EBCA) vs. T_r for the monomer LC solvent was found to be similar to those reported in our previous work,[6] and therefore not reproduced here.

In accordance with the previous analysis adopted for dimer CBA-n ($n = 9$, 10), the orientational correlation
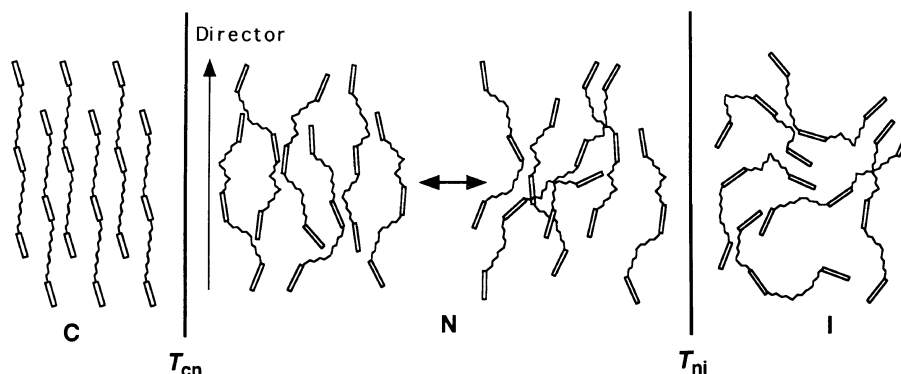
Figure 5. Schematic representation of the crystal–nematic and nematic–isotropic transitions, illustrated for a trimer LC system. The conformational distribution of the spacer remains quite stable in the nematic phase.

between CBA-T9 and EBCA molecules is shown in Figure 4, where the order parameter of the central biphenyl group S_{ZZ}^{M}(CBA-T9, central) derived by neglecting the biaxiality term is plotted against the order parameter S_{ZZ}^{M}(EBCA) of the coexisting monomer LC. The order parameter of the monomer is significantly higher than that of the trimer in the nematic mixture at any given temperature and concentration, indicating that spatial arrangements of the mesogens are largely restricted in the trimer due to the stereochemical requirement of the intervening spacer. These observations lead to a schematic diagram of the molecular arrangement in the nematic phase formed by CBA-T9 (Figure 5). The underlining principle for the spatial arrangement of the mesogenic units is essentially the same as that argued before.[6] For the dimers, efforts have also been made to elucidate the molecular arrangement in the LC state by employing other techniques such as the ^{13}C–^{13}C dipolar coupling and ^{13}C chemical shift anisotropy determination by ^{13}C NMR,[17] and the magnetic susceptibility measurements by SQUID.[18] All these studies favorably support the mesophase structure depicted above (Figure 5).

Estimation of Constant-Volume Transition Entropies from the PVT Data

The *V–T* measurements were performed in the isothermal mode, first by raising temperature at a 10 deg interval up to 280°C (Figure 6), and then continued in a similar manner during the cooling process. The specific volumes at zero pressure ($p=0$) were estimated from those observed at higher pressures: extrapolations were executed by using polynomial expressions. The extrapolated values are indicated by open circles in these diagrams. Since the *V–T* relation at $p=0$ involves extrapolation from higher pressures, the curves (open circles) often exhibit abnormal v_{sp} values around the NI transition region (*cf.* Figure 6).[6] An appreciable pressure dependence was observed for the phase transition temperatures (T_m and T_{ni}). In both samples, melting (T_m on heating) was observed at a higher temperature than crystallization (T_c on cooling). In contrast, the NI transition temperature remains nearly invariant for both heating and cooling process. The thermal expansion coefficients α and compressibilities β in the low-pressure region are the major interests in this work. The values estimated in the nematic and isotropic phases slightly
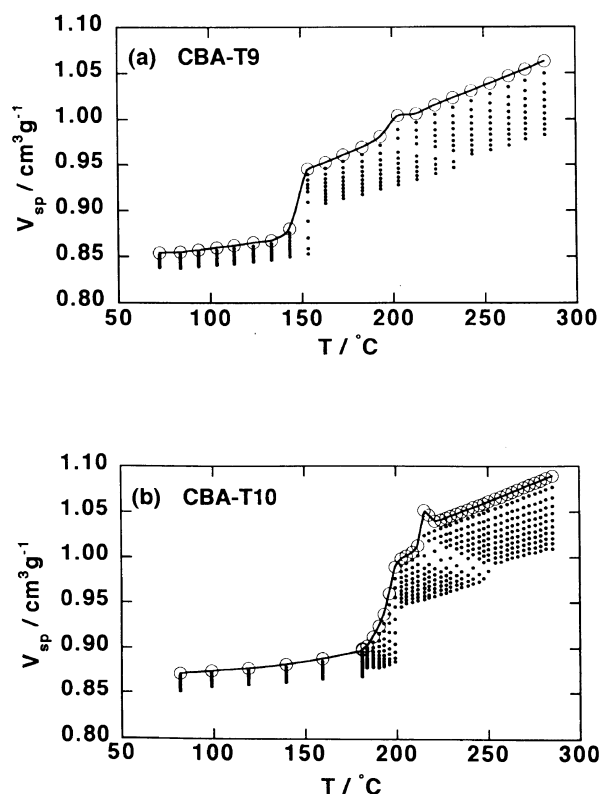

Figure 6. Volume *vs.* temperature relations for (a) CBA-T9 and (b) CBA-T10 from 10 to 100 MPa for each 10 MPa. Extrapolated values to zero pressure are indicated by open circles. For simplicity, v_{sp} / curves are drawn only for $p=0$.

above the transition temperature are listed in Table I, where T_m, T_c, and T_{ni} were taken to be the midpoint of the corresponding transitions indicated in the *V–T* diagram. The extrapolations of the experimental curves were carried out by using polynomial functions. The volume changes ΔV_{tr} at T_m, T_c, and T_{ni} can be obtained from the observed *V–T* relations. Variation of ΔV_{tr} with pressure observed during the heating and cooling process are illustrated in Figure 7, for CBA-T9 and -T10. While the volume change ΔV_{cn} at the CN transition tends to be moderately depressed as pressure increases, the corresponding transition volumes ΔV_{ni} at the NI interphase varies less sensitively with pressure for both samples.

The enthalpy changes under atmospheric pressure can be customarily measured by using DSC. The transition

Table I. Experimental values of ΔV_{tr}, $\alpha = (\partial \ln v_{sp}/\partial t)_p$ and $\beta = -(\partial \ln v_{sp}/\partial p)_t$ estimated in the low-pressure region for the nematic and isotropic states slightly above the transition temperature

Thermal process	Nematic state in the vicinity of T_m or T_c				Isotropic state in the vicinity of T_{ni}			
	T_m or T_c	ΔV_{cn}	$\alpha \times 10^3$	$\beta \times 10^3$	T_{ni}	ΔV_{ni}	$\alpha \times 10^3$	$\beta \times 10^3$
	°C	cm³ g⁻¹	K⁻¹	MPa⁻¹	°C	cm³ g⁻¹	K⁻¹	MPa⁻¹
				CBA-T9				
Heating	148	0.0705	0.90	0.54	200	0.0142	0.82	0.93
Cooling	142	0.0583	0.90	0.51	198	0.0162	0.81	0.83
				CBA-T10				
Heating	195	0.0915	0.75	0.57	214	0.0234	0.69	0.71
Cooling	192	0.0884	0.90	0.54	212	0.0220	0.76	0.77
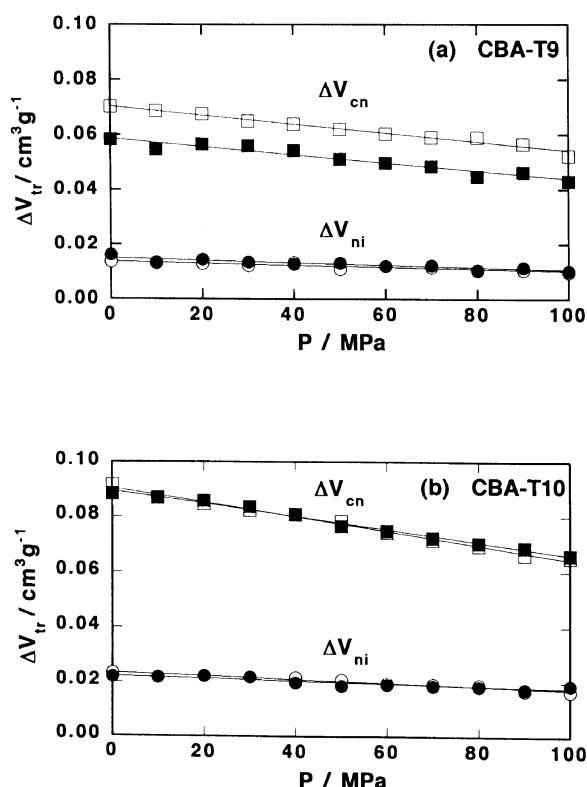
Figure 7. Variation of the transition volumes ΔV_{cn} (squares) and ΔV_{ni} (circles) as a function of pressure. The data points collected from the heating and cooling processes are distinguished respectively by open and filled symbols.

temperatures T_{cn} and T_{ni} and the heats ΔH_{tr} determined by DSC are given in Table II. The transition temperatures shown in the table are lower than those estimated previously from the V–T relation. Except for the crystallization temperature (T_c), differences between the DSC and PVT data are marginal. The values of ΔH_{tr} and the corresponding ΔS_{tr} were estimated by measuring the area of the DSC peaks in the usual manner. The observed values fluctuate within ± 10—15% around those listed in Table II.

The enthalpy changes may be alternatively estimated with the aid of the Clapeyron equation:

$$\Delta H_{tr} = T_{tr} \Delta V_{tr} dp/dt \qquad (4)$$

where dp/dt designates the slope of the phase boundary curve in the low-pressure region. For the NI transition, the values of dp/dt estimated from the measurements in

the isothermal and isobaric modes were mutually consistent. The enthalpy ΔH_{tr} and entropy changes ΔS_{tr} calculated according to eq 4 are listed in Table III. The difference between the PVT (Table III) and DSC methods (Table II) ranges between 5 and 45%. Following the previous treatment of dimers CBA-n, the values of ΔS_{ni} obtained by the PVT method and tabulated in Table III will be adopted for $(\Delta S_{ni})_p$ in the expression given in eq 1. As revealed in Figure 6, the observed CN phase boundary curves are less sensitive to the applied pressure, and the values of dp/dt estimated from these two figures inevitably include large uncertainties. The thermodynamic quantities such as ΔH_{cn} and ΔS_{cn} are therefore not included in Table III. In the following treatment, the values of $(\Delta S_{cn})_p$ for the CN transition were borrowed from the DSC measurements.

The values of ΔV_{tr}, γ, ΔS_v (*cf.* eq 2), and the transition entropies at constant volume $(\Delta S_{tr})_v$, defined as the difference between $(\Delta S_{tr})_p$ and ΔS_v in eq 1 are listed in Table IV, where the corresponding results obtained previously for dimer LCs (CBA-n) are also accommodated for comparison. Following our previous treatment, the values of the NI transition entropy for $p = 0$, $(\Delta S_{ni})_p$, were derived from the PVT data by using the Clapeyron relation. The changes in volume and entropy at the NI transition obtained for the mainchain dimer and trimer LCs are much larger than those reported for conventional monomer LCs.[19] The difference ΔT between the crystallization temperature T_c and the melting temperature T_m is sizable, especially in the DSC measurements, suggesting that supercooling takes place during crystallization. The enthalpy changes ΔH_{cn} observed during cooling may include some effect arising from this source. For the NI transition, the supercooling phenomenon is less marked, and thus the agreement between the heating and cooling processes is reasonable for the associated thermodynamic quantities. Although the precise estimation of errors involved in the elucidation of entropies is difficult, the uncertainties in the final results could amount to 30—40% of $(\Delta S_{ni})_v$.

The constant-volume transition entropies $(\Delta S_{tr})_v$ are expressed in terms of J mol⁻¹ K⁻¹. The entropies expressed by J(mole of spacers)⁻¹ K⁻¹ should be more appropriate in elucidating the role of the spacer in the individual systems. For trimers, these values are also listed in brackets. Comparison for given values of n yields a reasonable agreement between the CBA-n and CBA-Tn series, except for the case of $(\Delta S_{cn})_v$ for $n = 10$. Various

Table II. Summary of DSC data

Thermal process	CN transition			NI transition		
	T_{m} or T_{c}	ΔH_{cn}	ΔS_{cn}	T_{ni}	ΔH_{ni}	ΔS_{ni}
	°C	kJ mol^{-1}	J mol^{-1} K^{-1}	°C	kJ mol^{-1}	J mol^{-1} K^{-1}
			CBA-T9			
Heating	146.0	93.59	223.3	195.7	7.04	15.0
Cooling	129.9	90.62	224.9	193.7	7.64	16.4
			CBA-T10			
Heating	188.5	96.00	208.0	209.9	17.32	35.9
Cooling	159.3	82.69	191.2	205.9	20.76	43.3

Table III. Values of ΔH_{ni} and ΔS_{ni} derived from the Clapeyron relation[a]

Thermal process	T_{ni}	ΔV_{ni}	dp/dt	ΔH_{ni}[a]	ΔS_{ni}
	°C	cm^3 mol^{-1}	MPa K^{-1}	kJ mol^{-1}	J mol^{-1} K^{-1}
			CBA-T9		
Heating	200	11.7	2.13	11.8	25.0
Cooling	198	13.3	2.27	14.3	30.3
			CBA-T10		
Heating	214	19.9	2.50	24.3	49.8
Cooling	211	18.8	2.44	22.2	45.8

[a] $\Delta H_{\mathrm{tr}} = T_{\mathrm{tr}} \Delta V_{\mathrm{tr}} \mathrm{d}p/\mathrm{d}t$.

corroborations suggest that the value for the CBA-T10 sample may be underestimated to some extent.[20]

In our previous work,[3,4] a RIS simulation scheme was proposed to interpret the ^{2}H NMR quadrupolar splitting data observed in the LC state. On this basis, conformational entropy changes $\Delta S_{\mathrm{tr}}^{\mathrm{conf}}$ were estimated: $\Delta S_{\mathrm{cn}}^{\mathrm{conf}} = 59.6$ (CBA-9) and 64.2 (CBA-10), and $\Delta S_{\mathrm{ni}}^{\mathrm{conf}} = 13.3$ (CBA-9) and 15.6 (CBA-10), unit being J(mole of spacers)$^{-1}$ K^{-1}. These entropies correspond favorably with the values of $(\Delta S_{\mathrm{tr}})_v$ for both CBA-n and CBA-Tn series listed in Table I. The results suggest that the spatial configuration of the spacer is similar between the dimer and trimer for a given n in agreement with the spectroscopic observation mentioned above. The ensemble of conformers characterizing the nematic phase was previously termed nematic conformation.

Free Volume of the LC State

The free volume $f_v = (v - v^*)/v$ is a measure of fluidity of the system, where v^* designates the core volume. When the v^* values are estimated from the van der Waals volume of the constituent groups assembled in Bondi's Table[21] by assuming the additivity, the free volumes amount to $f_v \sim 0.40$, which is somewhat unrealistic. Free volumes may be estimated alternatively from an appropriate equation of state. Use of the Flory expression[22]

$$(v/v^*)^{1/3} - 1 = \alpha T/3(1 + \alpha T) \tag{5}$$

yields $f_v \sim 0.22$ for the isotropic melts of both dimers (CBA-n) and trimers (CBA-Tn) in the vicinity of T_{ni}. The core volume v^* estimated in this manner was found to be a little smaller than the specific volume of the cor-

responding crystals. Since the thermal expansion coefficient does not change much on going from the isotropic melt to the nematic LC state (*cf.* Table I), the free volume should remain nearly the same between these two states. The volume contraction at the I→N transition was found to be about 1/4 of the total volume change from the isotropic melt to the crystal. The dimer or trimer LC molecules are highly mobile in these nematic LC state.

CONCLUDING REMARKS

The results of the analysis on the dimer and trimer LCs presented above may be summarized as follows: (1) Under a uniaxial potential field, both spacer and mesogenic units at the terminals tend to align along the domain axis. Consequently the individual mesogenic cores inevitably incline to some extent with respect to the direction of molecular extension (*cf.* Figure 5), giving rise to a moderate value of the orientational order parameter S_{ZZ}^M. (2) As revealed by the studies of optical anisotropy[23] as well as magnetic susceptibility,[18] the molecular anisotropy of dimer compounds CBA-n ($n = 9$, 10) increases on going from the isotropic to the nematic LC state. Enhancement of the NI transition temperature may be largely caused by the intramolecular orientational correlation of the mesogenic units situated on both side of the spacer. Although the flexible spacer takes more extended conformation in the LC state, contribution of the spacer to the orientation-dependent intermolecular interactions seems to be small. (3) While the orientational fluctuation of the entire molecule varies as a function of temperature, the nematic conformation of the spacer remain nearly invariant over the entire range of the LC state. (4) It has been confirmed by the ^{2}H NMR and *PVT* studies that 50—60% of the transition entropy $(\Delta S_{\mathrm{tr}})_p$ arises from the variation in the conformational distribution of the spacer at the phase boundary.

In view of a relatively large free volume, it is reasonable to assume that the spacer is allowed to take all conformations except those strictly incompatible with the nematic environment. The disorientation angle of the terminal mesogens located on both sides of a spacer should provide a basis for such partition. Blumstein *et al.*'s observation[14] mentioned in the introductory part is consistent with the schematic view (Figure 5) presented in this paper. Finally, we wish to emphasize an important role of the flexible spacer in determining the molecular

Table IV. Estimation of the entropy change at constant volume for dimer CBA-n and trimer CBA-Tn with $n=9$ and 10

	CN transition				NI transition			
	ΔV_{cn}	γ	ΔS_v	$(\Delta S_{cn})_v{}^a$	ΔV_{ni}	γ	ΔS_v	$(\Delta S_{ni})_v{}^b$
	cm^3 mol^{-1}	MPa K^{-1}	J mol^{-1} K^{-1}	J mol^{-1} K^{-1}	cm^3 mol^{-1}	MPa K^{-1}	J mol^{-1} K^{-1}	J mol^{-1} K^{-1}
CBA-9	37.5	1.76	66.0	53.9 (81.0)^c	7.5	0.93	7.0	7.9 (8.3)^c
CBA-10	39.3	1.72	67.4	62.4 (76.4)^c	9.4	0.94	8.8	13.3 (11.6)^c
CBA-T9	58.1	1.67	97.1	126.2 [63.1]^d	11.7	0.88	10.3	14.7 [7.3]^d
CBA-T10	78.0	1.32	103.1	104.9 [52.4]^d	19.9	0.97	19.3	30.5 [15.3]^d

^{a} Estimated from the transition entropy determined by DSC measurements (Table II, heating process). ^{b} Estimated from the transition entropy determined by PVT measurements (Table III, heating process). ^{c} Estimated from the transition entropy determined by high pressure DTA measurements (ref 7). ^{d} unit: J(mole of spacers)$^{-1}$ K^{-1}.

ordering as well as thermodynamic properties of the mainchain-type LCs.

REFERENCES AND NOTES

1. A. Abe, *Macromol. Symp.*, **118**, 23 (1997).
2. A. Abe and S.-Y. Nam, *Macromolecules*, **28**, 90 (1995).
3. A. Abe, H. Furuya, R. N. Shimizu, and S.-Y. Nam, *Macromolecules*, **28**, 96 (1995).
4. A. Abe and H. Furuya, *Macromolecules*, **22**, 2982 (1989); A. Abe and H. Furuya, *Mol. Cryst. Liq. Cryst.*, **159**, 99 (1988); A. Abe, H. Furuya, and D. Y. Yoon, *Mol. Cryst. Liq. Cryst.*, **159**, 151 (1988).
5. K. Inomata, Ph.D Thesis, Tokyo Institute of Technology, 1991.
6. A. Abe, R. N. Shimizu, and H. Furuya, "Ordering in Macromolecular Systems", A. Teramoto, M. Kobayashi, and T. Norisuye, Ed., Springer, Berlin, 1994, pp 139—153.
7. Y. Maeda, H. Furuya, and A. Abe, *Liq. Cryst.*, **21**, 365 (1996).
8. J. W. Emsley, G. R. Luckhurst, G. N. Shilstone, and I. Sage, *Mol. Cryst. Liq. Cryst., Lett.*, **102**, 223 (1984).
9. A. Abe, *Macromolecules*, **17**, 2280 (1984).
10. L. Mandelkern, "Crystallization of Polymers," McGraw-Hill, New York, N.Y., 1964, Chapter 5.
11. The entropy separation according to eq 1 and 2 involves a hypothetical assumption that the volume of the isotropic fluid may be compressed to that of the mesophase, and successively from the mesophase to the crystalline state without affecting the configurational part of the entropy of chain molecules. The validity of such an assumption has been questioned in relation to polymer crystallization by several authors.[12] In a separate work,[13] we have extensively examined the volume dependence of thermal pressure coefficient γ for various chain molecules in the fluid state, where $\gamma=(\partial S/\partial V)_T$ designates the entropy change as

a function of volume at a given temperature. The results show that γ values are not much affected by the compression or expansion of the volume as long as the system remains highly fluid. It follows from that a simple expression set forth by eq 2 may be acceptable, or at least should not be excluded because of its simplicity, when the configurational entropy of chain molecules is estimated by the process described above.

12. B. Wunderlich and G. Czornyj, *Macromolecules*, **10**, 906 (1977); R. E. Robertson, *Macromolecules*, **2**, 250 (1969); M. Naoki and T. Tomomatsu, *Macromolecules*, **13**, 322 (1980); T. Bleha, *Polymer*, **26**, 1638 (1985), and references cited in these papers.
13. A. Abe, T. Takeda, and T. Hiejima, *Macromol. Symp.*, submitted.
14. R. B. Blumstein, E. M. Stickles, M. M. Gauthier, and A. Blumstein, *Macromolecules*, **17**, 177 (1984).
15. C. T. Imrie and G. R. Luckhurst, *J. Mater. Chem.*, **8**, 1339 (1998).
16. S.-Y. Nam, Ph.D Thesis, Tokyo Institute of Technology, 1994; A. Abe, T. Takeda, T. Hiejima, and H. Furuya, *Rep. Prog. Polym. Phys. Jpn.*, **40**, 261 (1997); T. Takada, A. Abe, T. Hiejima, and H. Furuya, *Kobunshi Ronbunshu*, **56**, 175 (1999).
17. R. N. Shimizu, H. Kurosu, I, Ando, A. Abe, H. Furuya, and S. Kuroki, *Polym. J.*, **29**, 598 (1997); R. N. Shimizu, N. Asakura, I. Ando, A. Abe, and H. Furuya, *Magn. Reson. Chem.*, **36**, S195 (1998).
18. H. Furuya, T. Dries, K. Fuhrmann, A. Abe, M. Ballauff, and E. W. Fischer, *Macromolecules*, **23**, 4122 (1990); H. Furuya, A. Abe, K. Fuhrmann, M. Ballauff, and E. W. Fischer, *Macromolecules*, **24**, 2999 (1991).
19. R. M. Stimpfle, R. A. Orwoll, and M. E. Schott, *J. Phy. Chem.*, **83**, 613 (1979).
20. C. Nakafuku, A. Abe, T. Takeda, and T. Hiejima, unpublished results obtained by using a high-pressure DTA.
21. A. Bondi, *J. Chem. Phys.*, **68**, 441 (1964).
22. P. J. Flory, R. A. Orwoll, and A. Vrij, *J. Am. Chem. Soc.*, **86**, 3607 (1964).
23. H. Furuya, S. Okamoto, A. Abe, G. Petekidis, and G. Fytas, *J. Phys. Chem.*, **99**, 6483 (1995).